AUTO-IGNITION MECHANISM NEAR THE BOUNDARY LAYER FOR HIGH-PRESSURE HYDROGEN RELEASE INTO CIRCULAR AND RECTANGULAR TUBES

Yokoyama, A.[1], Asahara, M.[2], Muto, D.[3] and Tsuboi, N.[4]

[1] Mechanical Engineering, Aoyama Gakuin University, 5-10-1 Fuchinobe, Chuo, Kanagawa, 252-5258, Japan, c5614112@aoyama.jp

[2] Mechanical Engineering, Aoyama Gakuin University, 5-10-1 Fuchinobe, Chuo, Kanagawa, 252-5258, Japan, asahara@aoyama.me.jp

[3] Department of Mechanical and Control Engineering, Kyushu Institute of Technology, 1-1 Sensui-cho, Tobata, Kitakyushu, Fukuoka, 804-8550, Japan, daiki.muto@gmail.com

[4] Department of Mechanical and Control Engineering, Kyushu Institute of Technology, 1-1 Sensui-cho, Tobata, Kitakyushu, Fukuoka, 804-8550, Japan, tsuboi@mech.kyutech.ac.jp

ABSTRACT

The accidents that hydrogen ignites without ignition source are reported in several cases, which phenomenon is called "auto-ignition." Since the use of high pressure hydrogen will be increased for the hydrogen society, it must be necessary to understand auto-ignition mechanism in detail to prevent such accidents. In this study we performed three-dimensional numerical simulations to clarify the auto-ignition mechanism using the three-dimensional compressive Navier-Stokes equations and a hydrogen chemical reaction model including nine species and twenty elementary reactions. We focus on the effects of the shape of the cross-section on the hydrogen auto-ignition mechanism applying for a rectangular and cylindrical tube. The results obtained indicate that the Richtmyer-Meshukov instability involves these auto-ignition.

1 INTRODUCTION

On March, 2014 the Tokyo Metropolitan Government (TMG) announced the policy that fuel-cell vehicles will be used to transport participants, officials, and staff at Tokyo Olympic and Paralympic Games, 2020. To guess from this policy, TMG decided to build a hydrogen society in Tokyo. Then as its start the hydrogen fuel-cell vehicles and hydrogen gas stations will be urgently and widely developed and constructed for transportation system. One of the advantages of the use of hydrogen is not to exhaust hydrocarbon micro-size particles during combustion. The characteristics of hydrogen gas are the high diffusion speed, high combustion speed, easy to leak, wide combustible mixture range, low ignition energy, and so on. Based on these hydrogen properties, hydrogen must be treated carefully. Hence it is important to set the safety standard of hydrogen to operate hydrogen station at any condition such as releasing the high pressure hydrogen to decrease its tank pressure and at any accident such as leaking of hydrogen gas because of the tank deterioration. It is reported that the high pressure hydrogen gas ignites in a tube without any ignition source when it is released through it. The phenomenon is called "auto-ignition" and must be studied for its cause and mechanism for its safety standard.

In 1972 Wolanski and Wojcicki [1] observed the auto-ignition phenomenon and reported that when the high pressure hydrogen was released into a cylindrical chamber through a pipe, which was filled with oxygen, an ignition occurred because of a shock wave heating at the condition that the hydrogen temperature was even lower than the auto-ignition temperature. Since their study, the flame at the exit of a tube obtained more attention and several different research were performed. In order to clarify the high pressure hydrogen auto-ignition mechanism in a tube, more studies were conducted: Dryer et al. [13] investigated the auto-ignition in the tube, which was not able to explain its reason. They released high pressure hydrogen into the air through the tube to find that the auto-ignition occurred by the temperature increase at the local position of the inside of the tube because the curved shock wave originated from the diaphragm burst reflected at the tube wall. In 2008 Wen et al. [14] reported by the numerical simulation that the combustible gas mixture yielded at the contact surface between hydrogen and air and the turbulent flow played an important role to promote the mixture gas in the tube. In 2009 Mogi et al. [6] obtained the following results from their experimental study that the auto-ignition occurred easier for the longer tube and higher tank pressure. Yamada et al. [17]

clarified numerically that the auto-ignition occurs near the tube wall because the vortex dynamics promotes the hydrogen chemical reactions to yield an auto-ignition (2009). Kitabayashi et al. [6] in 2010 performed the experiments using the longer tube to clarify that when the tube length is longer than 1.2 m, it is difficult for the hydrogen auto-ignition to occur. Recently in 2012 Kim et al. [19] performed their experiment using a rectangular tube to report that the auto-ignition occurred in the boundary layer in the tube because a mixing zone developed along the boundary layers to spread the ignition area over the mixing zone.

We can detect the auto-ignition in the tube, but it is difficult to clarify the location and the mechanism of hydrogen ignition and auto-ignition. This is because there are boundary layers near the visualizing windows, then the two-dimensional photos taken by Kim et al. [19] do not show the correct phenomena at the center of the tube. In order to clarify the auto-ignition phenomena, it is necessary to capture the detailed phenomena clearly.

In the present paper we will show the hydrogen auto-ignition mechanism inside the tube. Since it is difficult to observe the phenomenon experimentally and three-dimensionally, we perform the three-dimensional numerical simulation. Kim et al. [19] used a rectangular tube for their experiments to visualize the phenomenon through the window although a circular tube is used at the hydrogen station. So far we have not obtained any report to get a clear photo using the cylindrical tube. Hence the present study will provide the three-dimensional numerical analysis to simulate the experiments by Mogi et al. [6] and Kim et al. [19] to study the effects of the shape of the tube cross-section on auto-ignition in the tube.

2 NUMERICAL METHOD

The three-dimensional Navier-Stokes equations and the ones for the conservation of mass for each species are used as the governing equations of the present problem.

$$\frac{\partial \boldsymbol{Q}}{\partial t}+\frac{\partial \boldsymbol{E}}{\partial x}+\frac{\partial \boldsymbol{F}}{\partial y}+\frac{\partial \boldsymbol{G}}{\partial z}=\frac{\partial \boldsymbol{E_d}}{\partial x}+\frac{\partial \boldsymbol{F_d}}{\partial y}+\frac{\partial \boldsymbol{G_d}}{\partial z}+\boldsymbol{S}$$

$$\boldsymbol{Q}=\begin{pmatrix}\rho\\ \rho u\\ \rho v\\ \rho w\\ e\\ \rho_i\end{pmatrix},\ \boldsymbol{E}=\begin{pmatrix}\rho u\\ \rho u^2+p\\ \rho vu\\ \rho wu\\ (e+p)u\\ \rho_i u\end{pmatrix},\ \boldsymbol{F}=\begin{pmatrix}\rho v\\ \rho uv\\ \rho v^2+p\\ \rho wv\\ (e+p)v\\ \rho_i v\end{pmatrix},\ \boldsymbol{G}=\begin{pmatrix}\rho w\\ \rho uw\\ \rho vw\\ \rho w^2+p\\ (e+p)w\\ \rho_i w\end{pmatrix} \tag{1}$$

$$\boldsymbol{E_d}=\begin{pmatrix}0\\ \tau_{xx}\\ \tau_{xy}\\ \tau_{xz}\\ -q_x\\ \rho D_i\dfrac{\partial Y_i}{\partial x}\end{pmatrix},\ \boldsymbol{F_d}=\begin{pmatrix}0\\ \tau_{yx}\\ \tau_{yy}\\ \tau_{yz}\\ -q_y\\ \rho D_i\dfrac{\partial Y_i}{\partial y}\end{pmatrix},\ \boldsymbol{G_d}=\begin{pmatrix}0\\ \tau_{zx}\\ \tau_{zy}\\ \tau_{zz}\\ -q_z\\ \rho D_i\dfrac{\partial Y_i}{\partial z}\end{pmatrix},\ \boldsymbol{S}=\begin{pmatrix}0\\ 0\\ 0\\ 0\\ 0\\ \dot{\omega}_i\end{pmatrix}$$

where ρ – density, kg/m^3; u, v, w – velocity, m/s; e – energy, J/kg; ρ_i – density of each chemical specie, kg/m^3; p – pressure, Pa; τ – shearing stress, Pa; q – heat flux, J/kg; D – effective diffusion coefficient, m; Y – mass fraction, no dimension; $\dot{\omega}$ - preparation from chemical reaction, kg/m^3.

We employed the Strang-type time-splitting method for the unsteady terms, the Harten-Yee's second-order explicit non-MUSCL modified-flux-type total variation diminishing scheme for the convective terms, the second-order central difference scheme for the diffusion terms, and the point-implicit method for the production terms. The chemical reactions are calculated using the model by Hong et al. [26] which includes nine species of H_2, O_2, O, H, OH, HO_2, H_2O_2, H_2O, and N_2, and twenty elementary reactions. The transport coefficients are calculated using the Lennard-Jones model [27] and Wilke's law [10], respectively.

Figure 1-(a) shows the schematic grid system for the rectangular shock tube whose width and height are 10 mm and which are originally used in the experiments performed by Kim et al. [19]. The numerical length of the tube is 125 mm, which is shorter than the tube length used by Kim et al. [19], because we know that the auto-ignition occurs at the location shorter than 125 mm, which is observed experimentally and numerically. Besides the rectangular tube is vertically and horizontally symmetry so that we only need to calculate the area of its quarter cross section. The boundary conditions are non-slip or isothermal (300 K) wall conditions. The grid sizes of x-direction, y-direction, and z-direction are 50, 10, and 57 μm, respectively. The total number of the grid system is 2521 × 151 × 151. On the other hand, Figure 1-(b) shows the schematic grid system for the circular shock tube whose diameter is 10 mm and which is originally used for the experiments performed by Mogi et al. [6]. The numerical length of the tube is also 125 mm. The boundary conditions for this cylindrical tube are non-slip and isothermal (300 K) wall conditions. The grid size of r-direction and z-direction are 10 to 57μm, depending on the location of either near the wall or not. The circumferential direction of the grid interval is 3.0 degrees. The total grid number of the system is 2521 × 151 × 121. Since the circular tube has a curvature, there is a possibility that the influence of the boundary conditions in the case of calculating quarter region like the rectangular tube. Therefore, we calculate the all area of the circular tube. Table 1 shows the numerical conditions for the rectangular and cylindrical shock tube.

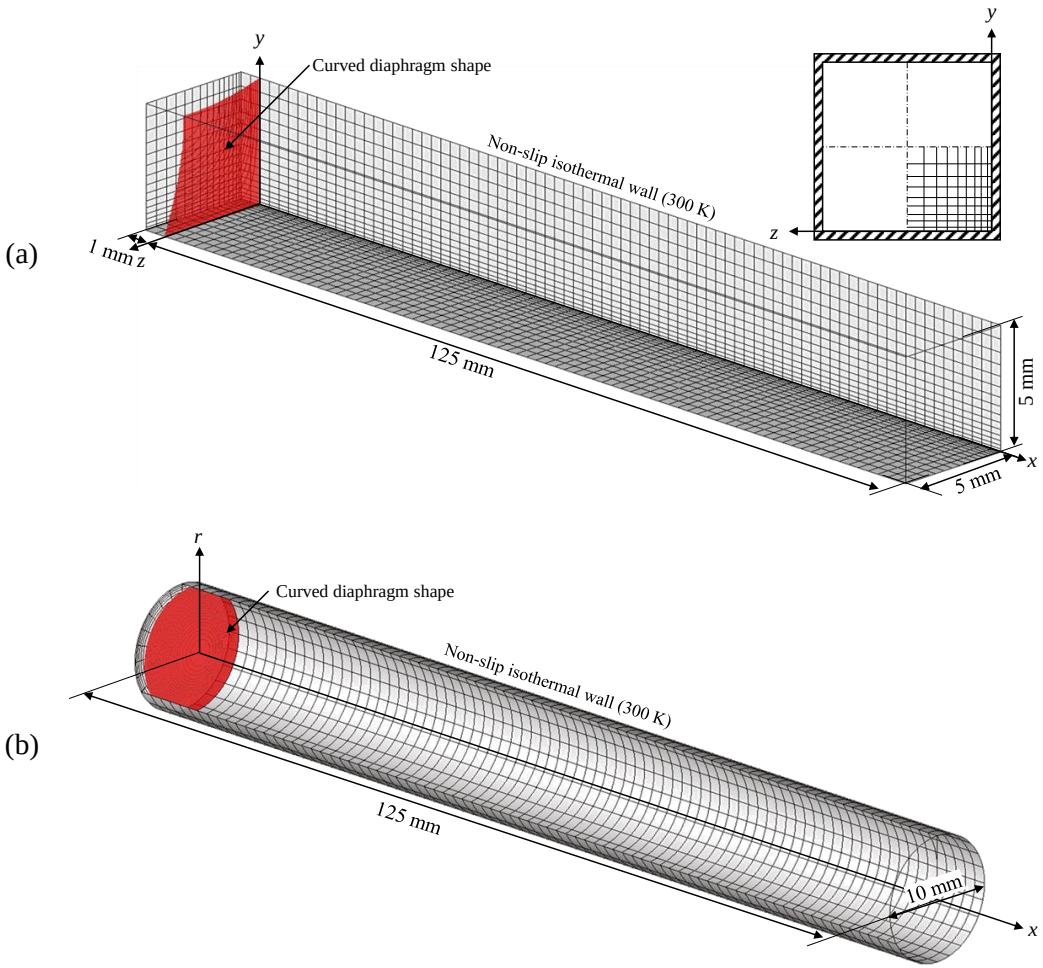

Figure 1. Numerical configuration of the present real size tubes system based on the rectangular tube used by Kim et al. [19] and circular tube used by Mogi et al. [6]

Table 1. Conditions of grid systems

	Rectangular tube	Circular tube
Grid number	2521×151×151	2521×151×121
Δx	50 μm	
Δy / Δr	10 – 57 μm	
Δz / $\Delta\ \theta$	10 – 57 μm	3.0 degree
Boundary condition	Non-slip isothermal condition (300 K)	

The initial conditions for the high pressure hydrogen are 9.0 MPa and 300 K and that for the air 0.1 MPa and 300 K. In addition, the high-pressure boundary is given by the fourth-order function by solving the bending problem of the elastic body with the distributed load. The process of rupturing diaphragm is ignored this time.

In the present study the area for ignition was investigated at the condition that hydrogen and air were mixed at the temperature of over 2400 K.

3 SIMULATION RESULTS AND THEIR DISCUSSION

3-1 VALIDATION OF CALCULATION

The time history of pressure is compared with the experimental results of Kim et al. [19] and Mogi et al. [6] and with the present simulation to study the validation of the results of the present numerical simulation. Besides the time history of the simulation is calculated using the size of the pressure sensors.

First of all we evaluate the results of the rectangular tube case. Kim et al. [19] installed eight pressure sensors which were located from the distance x of 57 mm by every 28 mm on the rectangular tube inner wall. They used the pressure sensors with the diameter of 6.3 mm (Kulite, ETM HT 375-5000G). In the present numerical simulation two pressure sensors are set. Figure 2 shows the time history of the pressure sensors p1 and p3 for the present numerical simulation and the experiments by Kim et al. [19]. Since the second pressure sensor of the experiment showed a lot of noises, we did not use its data in Figure 2. From Figure 2 the propagating speed of the leading shock wave is obtained from the pressure rises for both results of the experiment and the numerical simulation. The characteristic behaviors of vibrating pressure values of the numerical simulation shows qualitative agreement with that of the experiment. The pressure vibration probably comes from the transverse shock waves generated by diaphragm bursting. Since the high pressure hydrogen release and the pressure rises are slower in the experiments than that in the numerical simulation, the time history of the pressure profiles of the numerical simulation is a little higher than that of the experiments by Kim et al. [19].

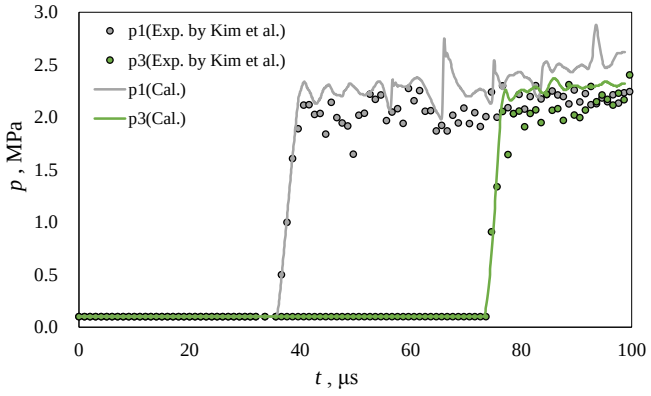

Figure 2. Time history of each pressure sensor in present simulation and the experiments performed by Kim et al. [19]

Secondly we evaluate the results of the cylindrical tube case. Mogi et al. [6] installed five pressure sensors which were located from the distance x of 50 mm by every 30 mm on the cylindrical tube inner wall. They used the pressure sensors with the diameter of 6.3 mm (PCB, Piezotronics 111A24). In the present numerical simulation three pressure sensors are set. Figure 3 shows the time history of the pressure sensors p1, p2, and p3 for the present numerical simulation and the experiments by Mogi et al. [6]. From Figure 3 the time of the pressure rise at p1 for the numerical simulation agrees well with that of the experimental data obtained by Mogi et al. The propagating speeds of the leading shock wave in this case are calculated from both data, but the pressure rises for p2 and p3 give some difference between the experimental data and the numerical ones; in other words, the numerical speed is faster than the experimental one.

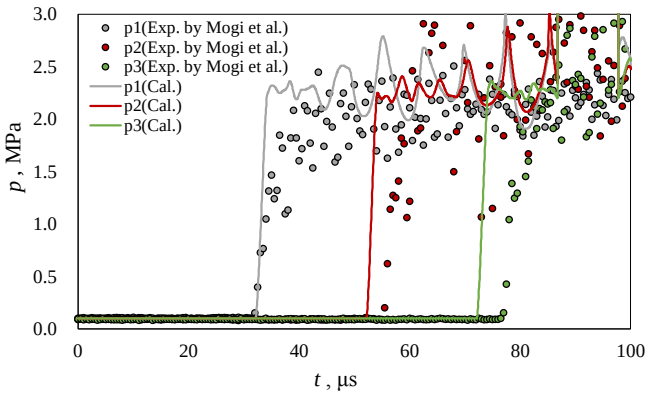

Figure 3. Time history of each pressure sensor in present simulation and the experiments performed by Mogi et al. [6]

From those comparisons between the experimental data and the numerical ones, the present simulation is valid to simulate the experiment and will be extended for the calculation of the further detailed cases.

3-2 PROPAGATING PROCESS IN RECTANGULAR TUBE

Figure 4 shows the propagation process of the high pressure hydrogen in the rectangular tube. Figure 4(a) presents the iso-surface of the hydrogen mass fraction of 0.1, which implies the contact surface of hydrogen and air. Figure 4(b) is the iso-surface of temperature at 2400 K, which implies the ignition region. And Figures 5 and 6 show the hydrogen mass fraction contours at the x-y (z=5.0 mm) cross-section and that at the y-z cross-section projected iso-surface, and the temperature contours at the x-y (z=5.0) cross-section and that at the y-z cross-section, respectively. At the time of 7.64 μs (Figures 5-(2) and 6-(2)), the auto-ignition occurs at the contact surface between hydrogen and air near the center of the wall. After the auto-ignition, the ignition region spreads at the time of 12.1 μs. Then new auto-ignition appears at the tube corner at the time of 17.1 μs (Figure 6-(4)). Looking at the iso-surface of the hydrogen mass fraction (t=17.1μs), the flow along the wall starts developing. The propagation speed of the ignition region from new auto-ignition is faster than that from the initial auto-ignition (t=7.64 μs). Finally the whole region of the contact surface becomes the igniting region at the time of 23.3 μs (Figures 4-(6) and 6-(6)). In summary two ignitions appears: one is at the wall center and another is at the tube corner.

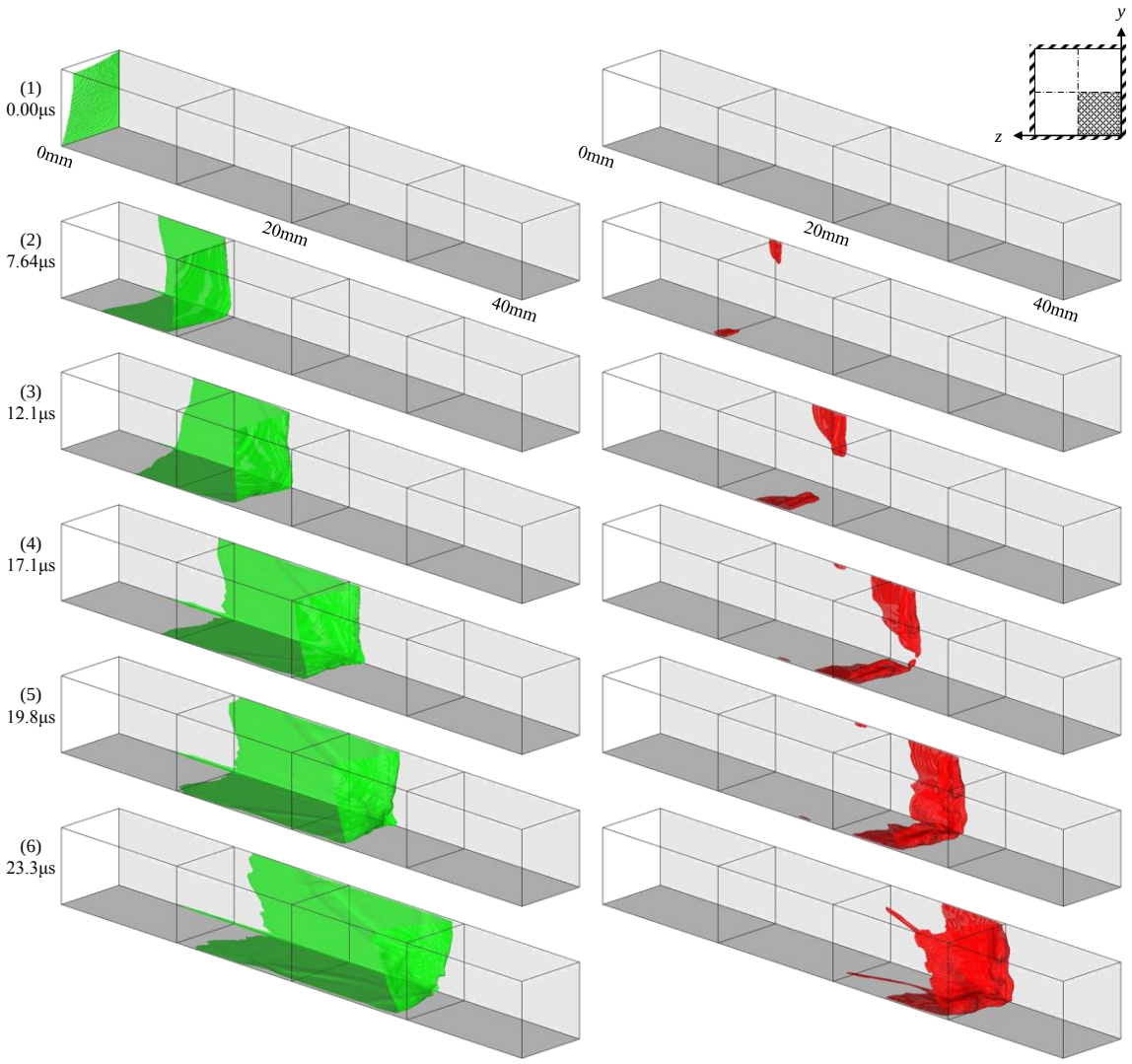

Figure 4. Iso-surface of hydrogen mass fraction equal to 0.1 in case of releasing to the rectangular tube, and iso-surface of temperature equal to 2400 K in case of releasing to the rectangular tube

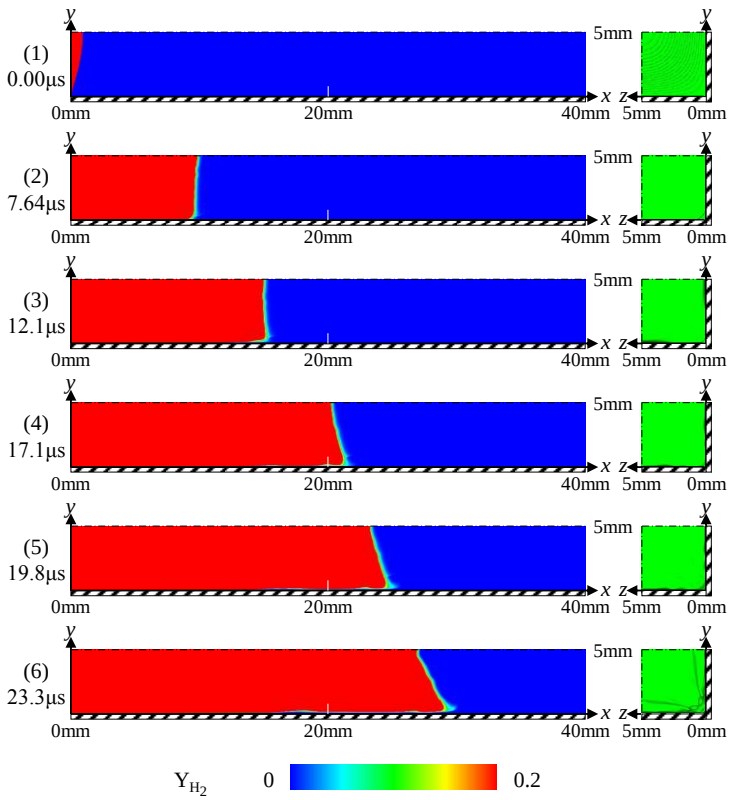

Figure 5. Contour of hydrogen mass fraction at the distance *z* of 5.0 mm and iso-surface seen from cross-section

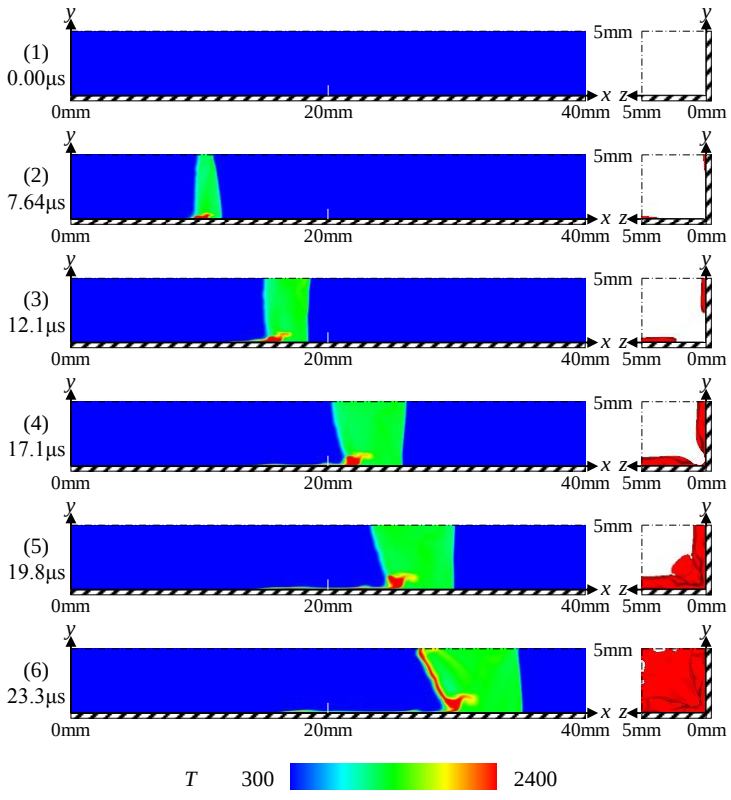

Figure 6. Contour of temperature at the distance *z* of 5.0 mm and iso-surface seen from cross-section

3-3 IGNITION MECHANISM

Figure 7 shows the flow structure when the high-pressure hydrogen is released to the rectangular tube. The leading shock wave comes out by bursting the diaphragm and the contact surface appears between hydrogen and air behind the leading shock wave. The air behind the leading shock wave and in front of the contact surface is heated. Besides, the air along the wall, behind the contact surface, and in the velocity boundary layer is heated high by the leading shock wave. Near the wall, hydrogen and the shock heated gas stratify along the wall and the transverse shock wave passes them. Then the vortices are generated by the Richtmyer-Meshukov instability and enhance mixing between hydrogen and the shock heated air. Finally the temperature of the mixture reaches the auto-ignition temperature to auto-ignite the mixture near the tube wall.

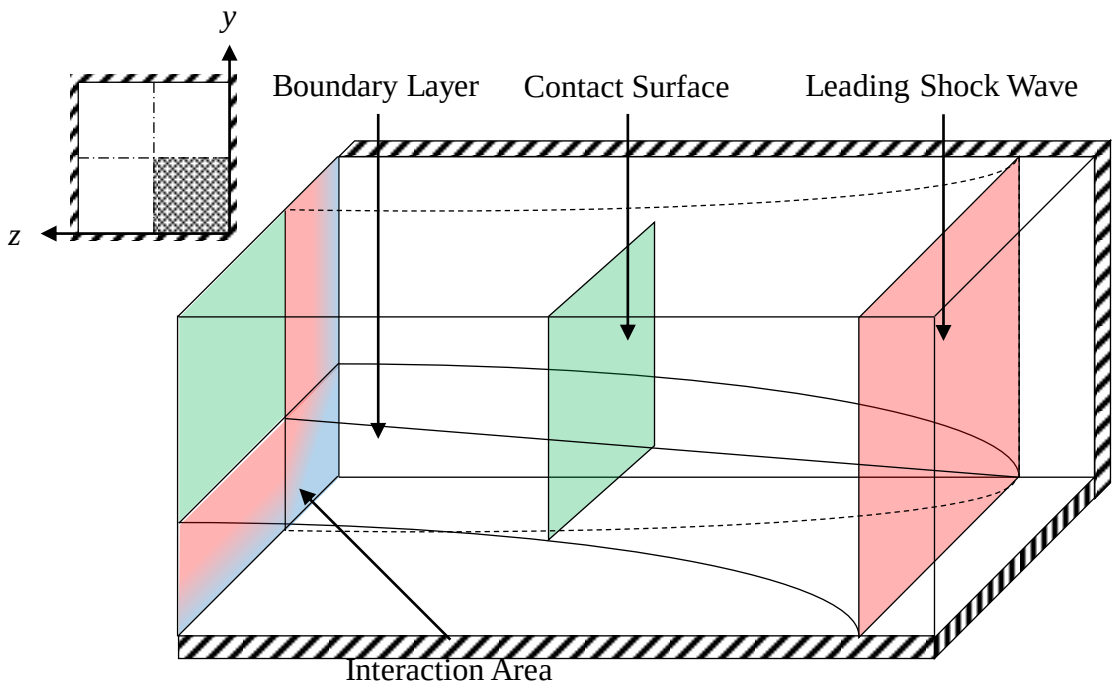

Figure 7. Structure of high-pressure hydrogen jet

New auto-ignition occurs at the tube corner because of the same auto-ignition mechanism described in the previous section. This auto-ignition at the tube corner has a property of longer ignition time then the initial auto-ignition and provides a faster flame propagation speed because the velocity boundary layers in the vertical wall and in the horizontal wall interact with each other at the tube corner. Then this interaction gives further to the other region. On the other hand, the temperature boundary layers developed from the vertical wall and horizontal wall interact with each other too. This interaction provides the tube corner temperature lower than the tube wall to give the region the longer auto-ignition time than the other region and to give the auto-ignition region wider.

3-4 PROPAGATING PROCESS IN CIRCULAR TUBE

Figure 8 shows the propagation process in the circular tube, where Figure 8(a) presents the iso-surface of the hydrogen mass fraction of 0.1 and Figure 8(b) does the iso-surface of temperature at 2400 K. Since all configurations in Figure 8 are line-symmetry, the quarter region of the tube is visualized. Figures 8 (a)-(2) and 8 (b)-(2) (t=6.48 μs) show the auto-ignition at the contact surface between hydrogen and air near the center of the wall. Then the ignition region spreads over gradually. Finally all contact surface region becomes the ignition region at the time of 40.0 μs (Figures 8(a)-(6) and 8 (b)-(6)). As a conclusion, only single ignition source exists in this case.

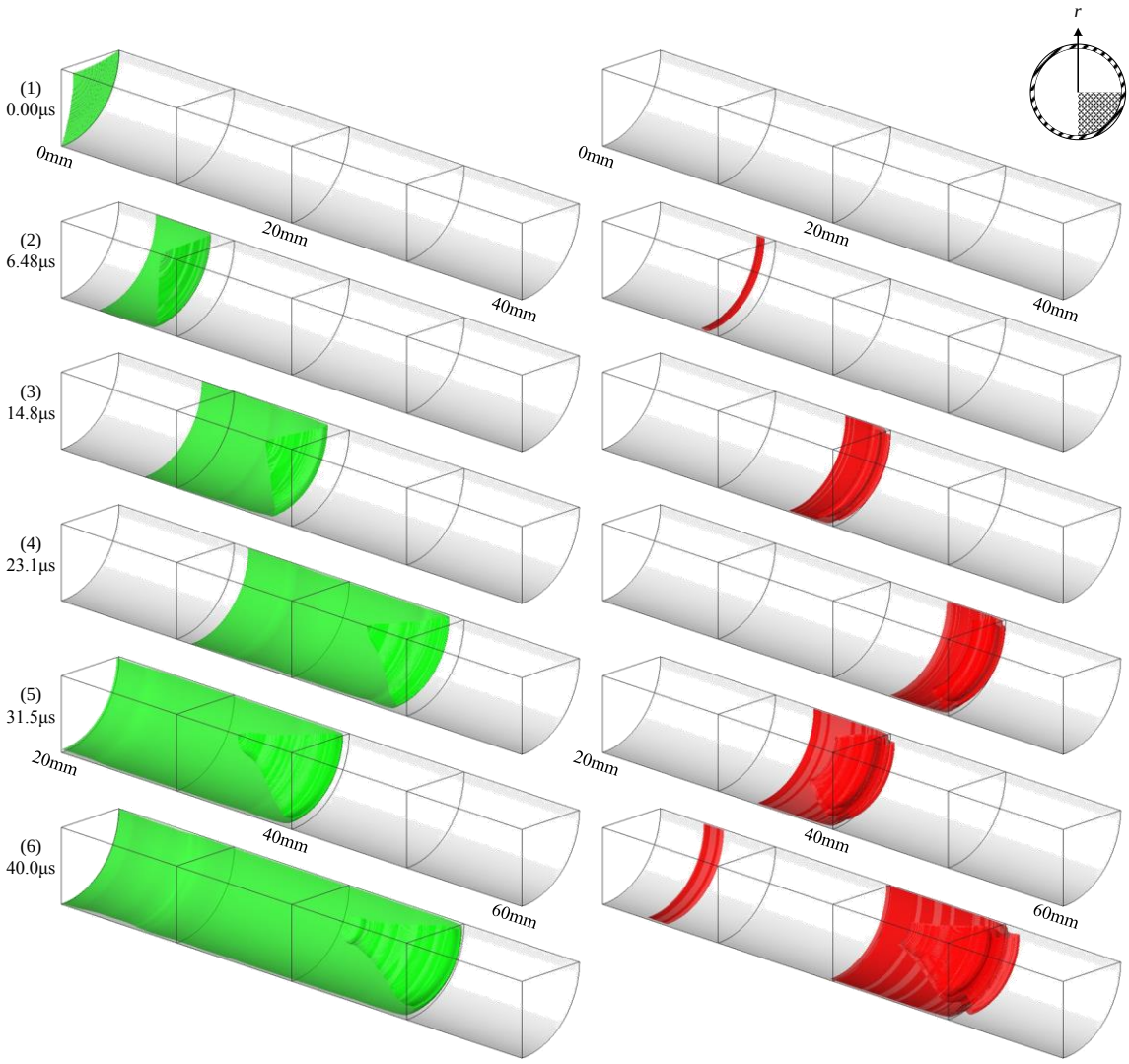

Figure 8. Iso-surface of hydrogen mass fraction equal to 0.1 in case of releasing to the circular tube, and iso-surface of temperature equal to 2400 K in case of releasing to the circular tube

3-5 COMPERING CONFIGURATION OF AUTO-IGNITION IN RECTANGULAR TUBE AND CIRCULAR TUBE

The configuration of auto-ignition is discussed for the rectangular and circular tube.

3-5-1 TIME HISTORY OF MAXIMAM TEMPERETURE

The time histories of the maximum temperature are compared with the initial auto-ignition time in Figure 9. In the figure the time history of the maximum temperature in the rectangular tube coincides with that in the circular tube. In the circular tube case the ring-shape ignition region is generated along the wall. However in the rectangular tube case the ignition region is produced only at the center of the tube wall because the temperature boundary layer along the wall affects the tube corner strongly. Although the shape of the ignition region in the rectangular tube is different from that of the circular tube, the time histories of the maximum temperature agree each other. Hence both initial ignition mechanisms are the same. In summary, the presence or absence of the auto-ignition does not depend on the shape of the tube cross-section.

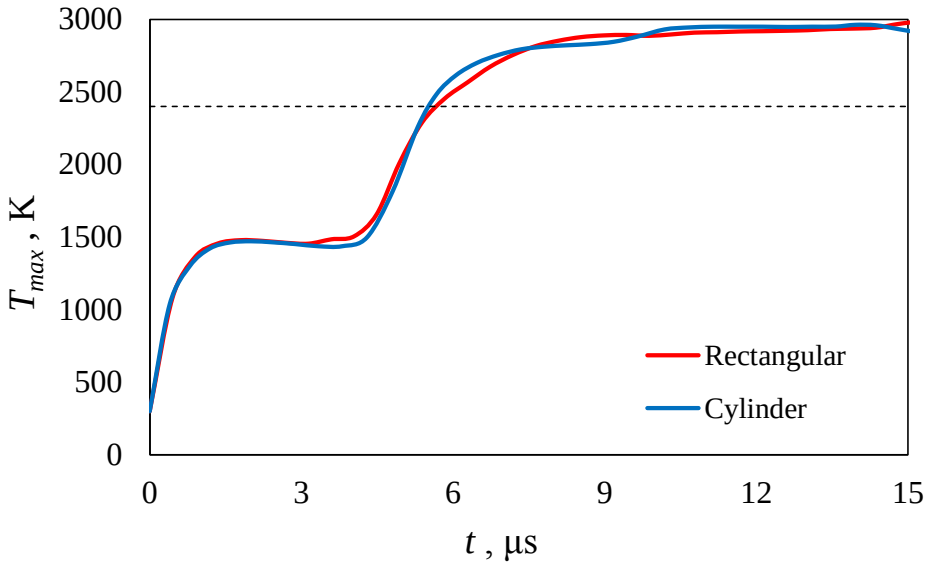

Figure 9. Time histories of maximum temperature each tube

3-5-1 TIME HISTORY OF THE IGNITION REGION VOLUME

The ignition region volume is calculated to compare with the time dependent ignition region volume which is spread to the whole contact surface. Figure 10 shows the time histories of the ignition region volume (V_{ign}). In addition, Figure 11 presents the time histories of the time differentiated ignition region volume, which implies the speed of the ignition region.

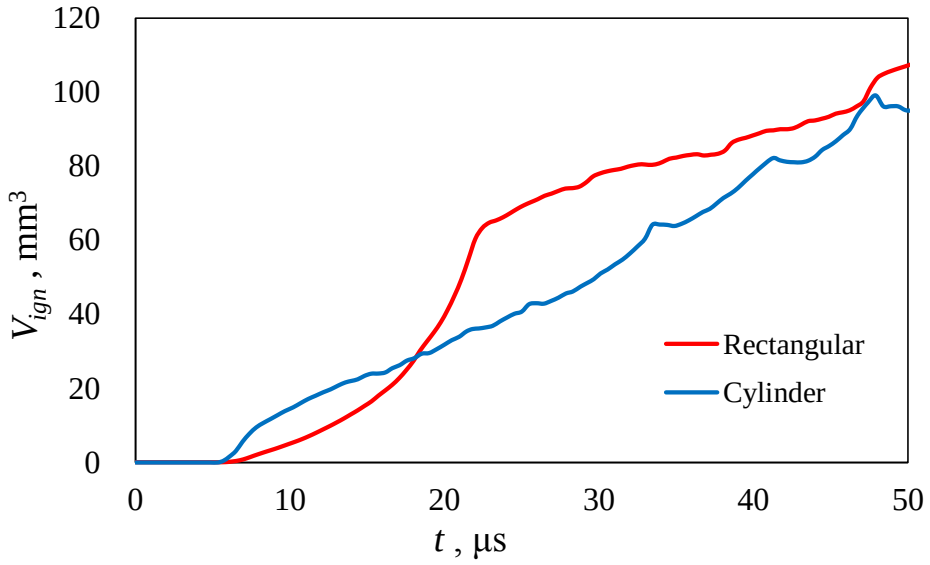

Figure 10. Time histories of the ignition region volume

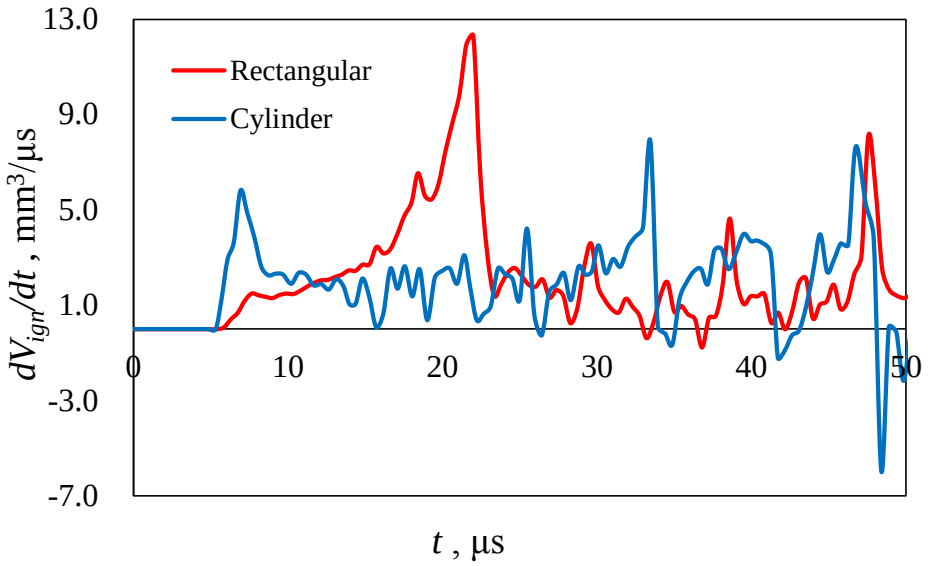

Figure 11. Time histories of time differentiated ignition area volume

The ignition region volume of the circular tube is larger than that of the rectangular tube up to 12.0 μs and before new auto-ignition occurs at the tube corner. From the time of 12.0 to that of 23.3 μs, the ignition region volume of the rectangular tube increases rapidly. Meanwhile the ignition region of the circular tube is rather constant through whole time history.

4 SUMMARY

In this paper, we performed three-dimensional numerical simulation for rectangular and circular tube to clarify the auto-ignition mechanism. So we can get below knowledge.

- Structure of auto-ignition in rectangular tube

First, initial auto-ignition occurs at the center of the tube wall. Second, new auto-ignition occurs at the tube corner. After that, ignition area spreads rapidly, and the whole of the contact surface becomes ignition area at 23.3 μs. The Richtmyer-Meshukov instability involves these auto-ignition. Additionally, the reason ignition gets delayed at the tube corner is the effects of boundary layer.

- Structure of auto-ignition in circular tube

There is only one ignition source near the wall, and the spreading speed of ignition area is constant. The whole of the contact surface becomes ignition area at 40.0 μs.

- Effects of cross sectional shape

We consider that the initial auto-ignition in case of the rectangular tube and auto-ignition in case of the circular tube are same mechanism from matching the time histories of maximum temperature. New auto-ignition at the tube corner is discriminative phenomenon from time histories of ignition area volume and time differentiated it.

5 ACKNOWLEDGMENT

This simulation used super computer system in Osaka University. We provided the experiments data by Mogi et al. [6] and Kim et al. [19]. We thank them.

1. Wolański, P. S. and Wójcicki, S., Investigation into the Mechanism of the Diffusion Ignition of a Combustible Gas Flowing into an Oxidizing Atmosphere, Proceedings of the Combustion. Institute, 14, 1973, pp. 1217-1223.

2. Golub, V.V., Baklanov, D.I., Bazhenova, T.V., Bragin, M.V., Glovastov, S.V., Ivanov, M.F., Volodin, V.V., Shock-induced Ignition of Hydrogen Gas During Accidental or Technical Opening of High-pressure Tanks, Journal of Loss Prevention in the Process Industries, 20, 2007, pp. 439-446.
3. Golub, V.V., Baklanov, D.I., Glovastov, S.V., Ivanov, M.F., Laskin, I.N., Saveliev, A.S., Semin, N.V., Volodin, V.V., Mechanisms of High-pressure Hydrogen Gas Self-ignition in Tubes, Journal of Loss Prevention in the Process Industries, 21, 2008, pp. 185-198.
4. Golub, V.V., Baklanov, D.I., Bazhenova, T.V., Glovastov, S.V., Ivanov, M.F., Laskin, I.N., Semin, N.V., Volodin, V.V., Experimental and Numerical Investigation of Hydrogen Gas Auto-ignition, International Journal of Hydrogen Energy, 34, 2009, pp. 5946-5953.
5. Mogi, T., Kim, D., Shiina, H., Horiguchi, S., Self-ignition and Explosion During Discharge of High-pressure Hydrogen, Journal of Loss Prevention in the Process Industries, 21, 2008, pp. 199-204.
6. Mogi, T., Wada, Y., Ogata, Y., Hayashi, A.K., Self-ignition and Flame Propagation if High Pressure Hydrogen Jets During Sudden Discharge From a Pipe, International Journal of Hydrogen Energy, 34, 2009, pp. 5810-5816.
7. Xu, B. P., Wen, J. X., Tam, V. H. Y., The Effect of an Obstacle Plate on the Spontaneous Ignition in Pressurized Hydrogen Release: A numerical study, 36, 2011, pp. 2637-2644.
8. Kitabayashi, N., Wada, Y., Mogi, T., Saburi, T., A.K. Hayashi, Experimental study on high pressure hydrogen jets coming out of tubes of 0.1 – 4.2 m in length, International Journal of Hydrogen Energy , Volume 38, 2013, pp. 8100-8107.
9. Xiaobo, S., Jinhua, S., Numerical Simulation on the Spontaneous Ignition of Leaking High Pressure Hydrogen from Terminal Unit, Physics Procedia, 33, 2012, pp. 8100-8107.
10. Bragin, M. V., Makarov, D. V., Molkov, V. V., Pressure Limit of Hydrogen Spontaneous Ignition in a T-shaped Channel, International Journal of Hydrogen Energy, 38, 2013, pp. 8039-8052.
11. Rudy, W., Dabkowski, A., Teodorczyk, A., Experimental and Numerical Study on Spontaneous Ignition of Hydrogen and Hydrogen-methane Jets in Air, 39, 2014, pp. 8039-8052.
12. Duan, Q., Xiao, H.,Gao, W., Wang, Q., Shen, X., Jiang, L., Sun, J., An Experimental Study on Shock Waves and Spontaneous Ignition Produced by Pressurized Hydrogen Release Through a Tube into Atmosphere, international Journal of Hydrogen Energy, 40, 2015, pp. 8281-8289.
13. Dryer, F.L, Chaos, M., Zhao, Z., Stein, J.N., Alpert, J.Y., Homer, C.J., Spontaneous Ignition of Pressurized Release of Hydrogen and Natural Gas into Air, Combustion Science and Technology, Volume 179, 2007, pp. 663-694.
14. Xu, B. P., Hima, L.I., Wen, J.X., Dembele, S., Tam, V.H.Y., Donchev, T., Numerical study on the spontaneous ignition of pressurized hydrogen release through a tube into air, Journal of Loss Prevention in the Process Industries, 21 (2), 2008, pp. 205-213.
15. Xu, B. P., Wen, J. X., Dembele, S., Tam, V. H. Y., Hauksworth, S. J., The Effect of Pressure Boundary Rupture Rate on Spontaneous Ignition of Pressurized Hydrogen Release, Journal of Loss Prevention in the Process Industries, 22, 2009, pp. 279-287.
16. Xu, B. P., Hima, L. I., Wen, J. X., Tam, V. H. Y., Numerical Study of Spontaneous Ignition of Pressurized Hydrogen Release into Air, 34, 2009, pp. 5945-5960.
17. Yamada, E., Watanabe, S., Hayashi, A. K., and Tsuboi, N., Numerical Analysis on Auto-ignition of a High Pressure Hydrogen Jet Spouting from a tube, Proceedings of the 32nd International Combustion Symposium, 32, 2009, pp. 2363-2369.
18. Yamada, E., Kitabayashi, N., Hayashi, A. K., Tsuboi, N., Mechanism of High Pressure Hydrogen Auto-ignition when Spouting into Air", International Journal of Hydrogen Energy, 36, 2010, pp.2560-2566.
19. Kim, Y.R., Lee, H.J., Kim, S.H., Jeung, I.S., A flow visualization study on self-ignition of high pressure hydrogen gas released into a tube, Proceedings of the Combustion Institute, 34, 2012, pp. 2057-2064.
20. Asahara, M., Yokoyama, A., Hayashi, A. K., Yamada, E., Tsuboi, N., Numerical Simulation of Auto-ignition Induced by High-pressure Hydrogen Release with Detailed Reaction Nodel: Fluid

Dynamic Effect by Diaphragm Shape and Boundary Layer, International Journal of Hydrogen Energy, 39, 2014, pp. 20378-20387.

21. Grune, J., Sempert, K., Kuznetsov, M., Jordan, T., Experimental Study of Ignited Unsteady Hydrogen Releases From a High Pressure Reservoir, International Journal of Hydrogen Energy, 39, 2014, pp. 20396-20403.
22. Morii, Y., Terashima, H., Koshi, M., Shimizu, T., Numerical study of the effect of obstacles on the spontaneous ignition of high-pressure hydrogen, Journal of Loss Prevention in the Process Insdustries, 34, 2015, pp. 92-99.
23. Strang, G., On the Construction and Composition of Difference Schemes, Society for Industrial and Applied Mathematics Journal on Numerical Analysis, 5, 1968, pp. 506-517.
24. Yee, H. C., Upwind and Symmetric Shock-Capturing Schemes, NASA Technical Memorandum, 89464, 1987.
25. Hong, Z., Davidson, D. F., Hanson, R. K., An Improved H_2/O_2 Mechanism Based on Recent Shock Tube: Laser Absorption Measurements, Combustion Flame, 158, 2011, pp. 633-644.
26. Chapman, S. and Cowling, T. G., The Mathematical Theory of Non-Uniform Gases, Cambridge University Press, 1970, pp. 226-259.
27. Wilke, C. R., A Viscosity Equation for Gas Mixtures, The Journal of Chemical Physics, 18, 1950, pp. 517-519.